



# Component-controllable cobalt telluride nanoparticles encapsulated in nitrogen-doped carbon frameworks for efficient hydrogen evolution in alkaline conditions



Hongxia Wang<sup>a,1</sup>, Yanwei Wang<sup>a,1</sup>, Lixing Tan<sup>c</sup>, Ling Fang<sup>a</sup>, Xiaohui Yang<sup>a</sup>, Zhengyong Huang<sup>b</sup>, Jian Li<sup>b</sup>, Huijuan Zhang<sup>a</sup>, Yu Wang<sup>a,b,\*</sup>

<sup>a</sup> The School of Chemistry and Chemical Engineering, and State Key Laboratory of Power Transmission Equipment and System Security, Chongqing University, 174 Shazheng Street, Shapingba District, Chongqing City, 400044, PR. China

<sup>b</sup> The School of Electrical Engineering, Chongqing University, 174 Shazheng Street, Shapingba District, Chongqing City 400044, PR. China

<sup>c</sup> Chongqing No. 1 Middle School, 2 Shanan Street, Shapingba District, Chongqing City 400030, PR. China

## ARTICLE INFO

### Keywords:

Cobalt telluride  
Tellurization process  
Nitrogen-doped carbon frameworks  
Hydrogen evolution reaction

## ABSTRACT

Rational structure design and component-controlled synthesis are attractive and challenging methods to develop materials with unique function for renewable energy conversion such as hydrogen production via water splitting. The earth-abundant and affordable transition metals have been regarded as ideal alternatives to precious platinum. Herein, we report the designed synthesis of component-modified cobalt telluride nanoparticles encapsulated in the nitrogen-doped carbon frameworks with the feature of high surface area and great electron conductivity. Compared with CoTe<sub>2</sub>/C and CoTe/C, the Co<sub>1.11</sub>Te<sub>2</sub>/C presents the highest catalytic activity for HER in 1M KOH due to its structural and component advantages. After a continuous reaction for 20 h or cycling for 1000 cycles, Co<sub>1.11</sub>Te<sub>2</sub>/C shows only a little performance loss. This work provides an effective approach to synthesize low-cost and efficient electrocatalysts for HER via rational structural and component design.

## 1. Introduction

With the rising environmental concerns and depletion of traditional fossil sources, the development of green and alternative energy has been a momentous demand [1–3]. Hydrogen, owing to its clean, renewable and high calorific value features, has been identified as the most potential and environmental-friendly energy to displace fossil fuels [4–7]. Among the various ways of producing hydrogen, water electrolysis is the most promising one which holds the merits of little pollution and high efficiency [8–10]. Platinum (Pt) is the best catalyst for the hydrogen evolution reaction (HER) since the Pt-H bond energy is related to supplying the fast HER reaction rate [11]. But its broad applications for the hydrogen economy are hampered by the scarce reserves on the earth and exorbitant price [3,12]. Hence, searching for active and non-Pt electrocatalysts has been an urgent task.

In recent years, many materials based on transition metal compounds, such as sulfides, [13,14] carbides [15–17], phosphides [18,19], metal alloys [20–22] and carbon-derived materials [23,24], have been widely explored as the earth-abundant catalysts. Especially, cobalt, as a

non-noble metal, has attracted great efforts to advance its catalytic activities for HER. For instance, Tian et al. [11] obtained CoP nanowire arrays and it displayed a low onset potential of 38 mV in acidic condition. CoS<sub>2</sub> [25] with diverse morphologies and CoSe<sub>2</sub> [26] with different phases, which are prepared by Faber et al. and Zhang et al. respectively, both exhibited good performance for HER. Most of the Co-based catalysts exhibit great performance under acidic condition but lack high activities in alkaline media [27–29]. Nevertheless, to obtain high purity hydrogen and reduce the acid-fog pollution, alkaline water electrolysis has great potential in large-scale industrialization as an appealing alternative to proton exchange membrane technology [30,31]. Herein, the development of HER catalysts with low overpotential and high stability in alkaline media is still challenging.

Cobalt telluride materials have been reported to serve as high active and stable electrocatalysts for HER, [32–34] oxygen evolution reaction (OER) [35,36], oxygen reduction reaction (ORR) [37] and other electrochemical applications [38–40]. Owing to the outstanding metallic characteristic in comparison with congeners including O, S and Se, tellurium, which has good electronic conductivity, contributes to high

\* Corresponding author.

E-mail address: [wangy@cqu.edu.cn](mailto:wangy@cqu.edu.cn) (Y. Wang).

<sup>1</sup> Hongxia Wang and Yanwei Wang contributed equally to this work.

electrocatalytic activity [36,41]. Although the previous studies have reported the successful synthesis of cobalt telluride with different Co/Te ratio, including  $\text{CoTe}_2$  [32],  $\text{Co}_{1.67}\text{Te}_2$  [37],  $\text{CoTe}$  [38] etc, an impartial comparison of their HER performance in basic media have not been investigated. However, component modification with different atom ratio in a proper range is an efficient strategy to improve the catalytic activity of electrocatalysts through adjusting the electronic structure. Callejas et al. [42] have reported that  $\text{Co}_2\text{P}$  nanoparticles show better performance for HER compared with equivalent  $\text{CoP}$ . The HER activities of crystalline  $\text{NiS}$ ,  $\text{NiS}_2$  and  $\text{Ni}_3\text{S}_2$  nanoparticles have been verified to lead the order of  $\text{Ni}_3\text{S}_2 > \text{NiS}_2 > \text{NiS}$ . [43] These works strongly demonstrate the practical significance of component modification in improving the performance of HER. Besides tuning the chemical composition, utilizing the conductive substrates carried on the specific nanostructure materials is also a key approach to enhance electrochemical performance. S. Damyanova et al. have proved that choosing the appropriate texture and texture components has important influence on the dispersion of active materials and the interaction between active materials and substrates, further improving the catalytic activity [44]. Recently, metal-organic frameworks (MOFs), which are consisted of central metal ions and organic linkers, have attracted widely attention as the conductive and heteroatom doped substrates and precursors [45–49]. Owing to their porous features and large surface area, the anchored functional materials could expose plenty active sites to promote the performance of electrocatalysts. For instance,  $\text{CoP}$  embedded N-doped carbon nanotube frameworks, which is synthesized from the MOF precursor, has been reported to exhibit good performance for the HER [50]. Otherwise, the intrinsic structure of MOFs could protect the active nanostructure catalysts from aggregation, improving the stability and durability of catalysts aimed to function well for long period of reaction.

Herein, we report a series of nitrogen-doped mesoporous organic frameworks encapsulated component-modified cobalt telluride nanoparticles (including  $\text{CoTe/C}$ ,  $\text{Co}_{1.11}\text{Te}_2/\text{C}$  and  $\text{CoTe}_2/\text{C}$  respectively) through a facile strategy. Remarkably, we firstly synthesize  $\text{Co}_{1.11}\text{Te}_2$  nanostructures via a chemical vapor deposition (CVD) method. The composition of cobalt telluride can be controlled by synthetic temperature and different molar ratios of Co-based precursor and Te power. Co-based carbon frameworks (ZIF-67) are taken as precursors and become graphitized at the temperature of tellurization. There is a crucial synergistic effect between N-doped carbon templates and active nanoparticles in the process of electrochemical reaction. The  $\text{Co}_{1.11}\text{Te}_2/\text{C}$  exhibits the better HER performance with the lower overpotential and Tafel slope in 1 M KOH, compared with  $\text{CoTe/C}$  and  $\text{CoTe}_2/\text{C}$ . The unique electronic structure of  $\text{Co}_{1.11}\text{Te}_2/\text{C}$  enhance the HER activity.

## 2. Experimental section

### 2.1. Materials

All chemicals, including cobalt nitrate hexahydrate, tellurium powder, 2-methylimidazole and methanol, were bought from Aladdin or Chengdu Kelong Chemical Reagent Factory and used without further purification.

### 2.2. Synthesis of ZIF-67 precursors

ZIF-67 precursors were prepared in accordance with reported references. Typically, 985.2 mg (12 mmol) 2-methylimidazole and 582 mg (3 mmol) cobalt nitrate hexahydrate  $\text{Co}(\text{NO}_3)_2 \cdot 6\text{H}_2\text{O}$  were dissolved in 35 ml of methanol, respectively, gently stirring for ten minutes. Then the 2-methylimidazole solution was rapidly added into  $\text{Co}(\text{NO}_3)_2$  solution and stirred for 15 min. The mixed solution was aged (incubated) at room temperature for 24 h. The obtained precipitates ZIF-67 were collected by centrifugation and washed with absolute ethanol for three times. Finally, the resulting product was dried at 60 °C

in vacuum for further use.

### 2.3. Synthesis of $\text{CoTe}_2/\text{C}$ , $\text{Co}_{1.11}\text{Te}_2/\text{C}$ and $\text{CoTe/C}$

The above synthesized ZIF-67 precursors were further annealed with Te powder under Ar atmosphere. 50 mg ZIF-67 and 100 mg Te power were separately put into two graphite boats and annealed at 680 °C for 60 min at a ramp rate of 5 °C min<sup>-1</sup> to obtain  $\text{CoTe}_2/\text{C}$ .  $\text{Co}_{1.11}\text{Te}_2/\text{C}$  and  $\text{CoTe/C}$  were prepared by a similar method. 50 mg ZIF-67 and 100 mg Te power were annealed at 720 °C and 780 °C for 60 min to synthesize  $\text{Co}_{1.11}\text{Te}_2/\text{C}$  and  $\text{CoTe/C}$ , respectively.

### 2.4. Synthesis $\text{Co}_{1.11}\text{Te}_2$ powder

To prepare  $\text{Co}_{1.11}\text{Te}_2$  powder, we first annealed as-prepared ZIF-67 precursors for 6 h under 500 °C in air atmosphere to obtain  $\text{Co}_3\text{O}_4$  powder. Then 50 mg  $\text{Co}_3\text{O}_4$  powder and 100 mg Te power were separately put into two graphite boats and annealed at 700 °C for 2 h in Ar atmosphere in order to get final  $\text{Co}_{1.11}\text{Te}_2$  powder.

### 2.5. Materials characterization

The morphologies and structures of as-prepared samples were examined by a field-emission scanning electron microscope (SEM, JEOL JSM-7800 F) which is coupled with an EDS analyzer (1Te<sub>2</sub> nanoparticles with small size.

X-ray photoelectron spectroscopy (XPS) was further applied to investigate the elemental composition and chemical states of the prepared samples. XPS survey spectra of  $\text{Co}_{1.11}\text{Te}_2/\text{C}$ ,  $\text{CoTe}_2/\text{C}$  and  $\text{CoTe/C}$  in Fig. 2b show that the surface of  $\text{Co}_{1.11}\text{Te}_2/\text{C}$ ,  $\text{CoTe}_2/\text{C}$  and  $\text{CoTe/C}$  are composed of Co, Te, C, N and O in accordance with their distinct peaks. The high-resolution XPS peaks of Co 2p are illustrated in Fig. 2c, showing that the peaks of  $\text{Co}_{1.11}\text{Te}_2/\text{C}$   $\text{CoTe}_2/\text{C}$  and  $\text{CoTe/C}$  centered at 780.8 eV (± 0.1 eV) and 796.8 eV (± 0.1 eV) are concordant with the binding energy of  $\text{Co 2p}_{3/2}$  and  $\text{Co 2p}_{1/2}$ . The peaks of  $\text{Co 2p}_{3/2}$  verify the existence of Co-Co bond, while the peaks of  $\text{Co 2p}_{1/2}$  suggest the presence of  $\text{Co}^{2+}$  in cobalt telluride. Two satellite peaks are located at 802.9 eV and 786.6 eV, which can be attributed to the surface oxidized  $\text{CoO}_x$ , further proving the existence of O in the survey scan. The peaks at the bonding energy of 778 eV are attributed to metallic Co. As is shown in Fig. 2d, the high-resolution XPS peaks of Te 3d are centered at 586.4 eV (± 0.1 eV) and 576.0 eV (± 0.2 eV), corresponding to the  $\text{Te 3d}_{3/2}$  and  $\text{Te 3d}_{5/2}$ , respectively [36]. The remaining two peaks at the binding energy of 583.4 eV (± 0.1 eV) and 572.9 eV (± 0.2 eV) indicate the presence of zero valent Te. After high-temperature annealing process, a small amount of tellurium vapor was deposited on the surface of the catalyst as zero valent Te during the cooling down process. The C 1s XPS peaks at 286.4 eV, 285.8 eV and 284.8 eV (Fig. S7a–c) are assigned to C–O, C–N/C=N and C–C bonds, respectively [55]. The peaks of N 1s (Fig. S7d–f) located at 401.0 eV, 399.7 eV and 398.8 eV, corresponding to the bonding energy of N in different chemical states. In order to discuss the synergistic effect between N-doped Carbon substrates and cobalt tellurium, the XPS spectrum of pure  $\text{Co}_{1.11}\text{Te}_2$  powder was measured. As is shown in Fig. S8a, the peaks of Co 2p of  $\text{Co}_{1.11}\text{Te}_2/\text{C}$  shifted to a higher binding energy compared with that of  $\text{Co}_{1.11}\text{Te}_2$  powder, which may be caused by the electron transfer between substrates and cobalt telluride. This result confirms the interaction between N-doped Carbon substrates and  $\text{Co}_{1.11}\text{Te}_2$  nanoparticles. From Fig. S8b, we can see that XPS survey spectra of  $\text{Co}_{1.11}\text{Te}_2$  powder don't show the obvious peaks of N, proving that  $\text{Co}_{1.11}\text{Te}_2$  powder is pure without N-doped carbon. What's more, Fig. 3a displays the  $\text{H}_2$ -TPR profiles of  $\text{Co}_{1.11}\text{Te}_2/\text{C}$ ,  $\text{CoTe}_2/\text{C}$  and  $\text{CoTe/C}$ . Each sample exhibits a major peak in the temperature range of 350–410 °C, which is ascribed to the reduction of  $\text{Co}^{3+}/\text{Co}^{2+}$  to  $\text{Co}^0$  [51–54,56]. With the increment of Co/Te ratio, the peak of samples shifted to a higher temperature, indicating that the reducibility of catalysts can be adjusted by

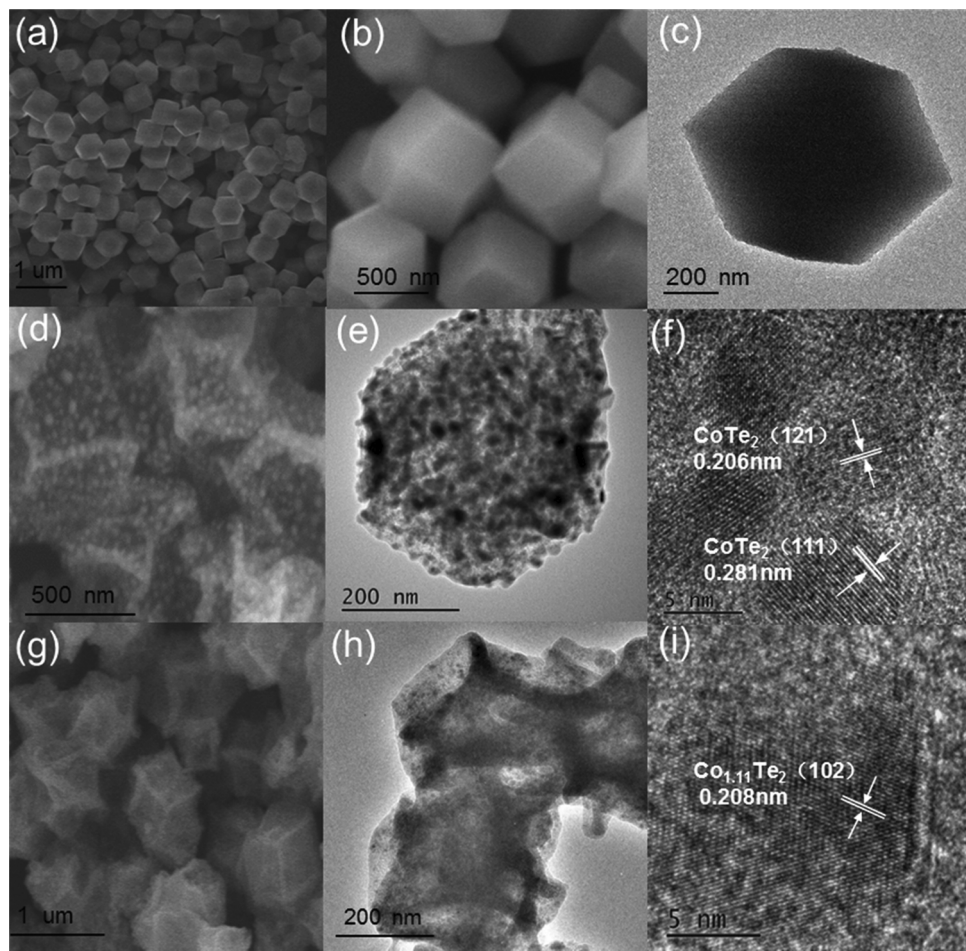


**Fig. 1.** Low- and high-magnification SEM images of ZIF-67 (a), (b); TEM images of ZIF-67 (c); Low-magnification SEM images of CoTe<sub>2</sub>/C and Co<sub>1.11</sub>Te<sub>2</sub>/C (d), (g); low and high-magnification TEM images of CoTe<sub>2</sub>/C (e), (f) and Co<sub>1.11</sub>Te<sub>2</sub>/C (h), (i).

component modification and three catalysts possess different interaction. Although the weight percentage of cobalt in the samples increased with the order of CoTe<sub>2</sub>/C < Co<sub>1.11</sub>Te<sub>2</sub>/C < CoTe/C, Co<sub>1.11</sub>Te<sub>2</sub>/C has the highest hydrogen consumption (146.7  $\mu\text{mol g}^{-1}$  cat) compared with that of CoTe<sub>2</sub>/C (74.5  $\mu\text{mol g}^{-1}$  cat) and CoTe/C (95.5  $\mu\text{mol g}^{-1}$  cat). This result suggested the existence of more reducible Co species in Co<sub>1.11</sub>Te<sub>2</sub>/C and high surface dispersion of Co ions.

The composition of the products can also be characterized by the Raman spectra. Fig. S9 demonstrates the Raman spectra of Co<sub>1.11</sub>Te<sub>2</sub>/C, CoTe<sub>2</sub>/C and CoTe/C in accordance with red, green and blue line, respectively. The peaks observed at 1340  $\text{cm}^{-1}$  ( $\pm 10 \text{ cm}^{-1}$ ) and 1380  $\text{cm}^{-1}$  ( $\pm 10 \text{ cm}^{-1}$ ) are derived from the D bond and G bond of the carbon, respectively, corresponding to the  $\text{sp}^3$  defect sites and  $\text{sp}^2$ -bonded pairs, which suggest the formation of structure defects and graphitic carbon in the calcined process. The graphitic carbon contributes to improve the electron transfer while structure defects could greatly enhance the electron donor-acceptor ability in the electrocatalysis process. Brunauer–Emmett–Teller (BET) method is used to evaluate the intrinsic feature of as-prepared catalysts including the specific surface area and pore size distribution. From Fig. 3b–d, we can clearly see that Co<sub>1.11</sub>Te<sub>2</sub>/C, CoTe<sub>2</sub>/C and CoTe/C all present a type IV N<sub>2</sub> adsorption-desorption isotherm with a H<sub>3</sub>-type hysteresis loop at the relative pressure (from 0.43 to 1 P/P<sub>0</sub>), revealing the nature of mesopores. To further obtain the pore-size information, the Barrett–Joyner–Halenda (BJH) measurement was carried out. The pore size distribution curve of Co<sub>1.11</sub>Te<sub>2</sub>/C shows a narrow peak at about 3.75 nm, which is similar with those of CoTe<sub>2</sub>/C (3.78 nm) and CoTe/C (3.74 nm). Furthermore, according the BET equation, the surface area

of Co<sub>1.11</sub>Te<sub>2</sub>/C, CoTe<sub>2</sub>/C and CoTe/C is calculated to be 110.4  $\text{m}^{-2} \text{ g}^{-1}$ , 109.1  $\text{m}^{-2} \text{ g}^{-1}$  and 51.8  $\text{m}^{-2} \text{ g}^{-1}$ , respectively. The above results reveal that Co<sub>1.11</sub>Te<sub>2</sub>/C possesses large surface area and high porosity, which are helpful to increase the contact area between the catalyst and electrolyte and decrease the local electrical resistance and dielectric constant, thus improving the electrocatalytic performance for HER [57].

## 2.6. Electrocatalytic activities for HER

The electrocatalytic HER performance of as-synthesized Co<sub>1.11</sub>Te<sub>2</sub>/C was assessed in 1 M KOH solution using a three-electrode system (details can be seen in experimental section). For comparison, CoTe<sub>2</sub>/C, CoTe/C and Pt/C were also measured at the same conditions. The linear sweep voltammetry (LSV) curves of Co<sub>1.11</sub>Te<sub>2</sub>/C, CoTe<sub>2</sub>/C, CoTe/C and Pt/C are demonstrated in Fig. 4a. As expected, Pt/C shows great catalytic activity for HER with an onset overpotential of about zero, corresponding to the reported work. Obviously, Co<sub>1.11</sub>Te<sub>2</sub>/C possesses better HER activity than CoTe<sub>2</sub>/C and CoTe/C with much earlier onset overpotential and higher current density. As is shown in Fig. 4b, Co<sub>1.11</sub>Te<sub>2</sub>/C shows a lower overpotential of 178 mV than that of CoTe<sub>2</sub>/C and CoTe/C with 295 mV and 397 mV at the current density of 10 mA  $\text{cm}^{-2}$ , respectively. In addition, the LSV curve of Co<sub>1.11</sub>Te<sub>2</sub> powder was also measured to compare with that of Co<sub>1.11</sub>Te<sub>2</sub>/C (Fig. S10). As observed, the catalytic activity of Co<sub>1.11</sub>Te<sub>2</sub> powder exhibits an obvious loss in comparison with that of Co<sub>1.11</sub>Te<sub>2</sub>/C, which shows a 37 mV decrease for the overpotential at the current density of 10 mA  $\text{cm}^{-2}$ , suggesting that the N-doped carbon templates of Co<sub>1.11</sub>Te<sub>2</sub>/C are able to improve the catalytic performance. Due to the porous characteristics

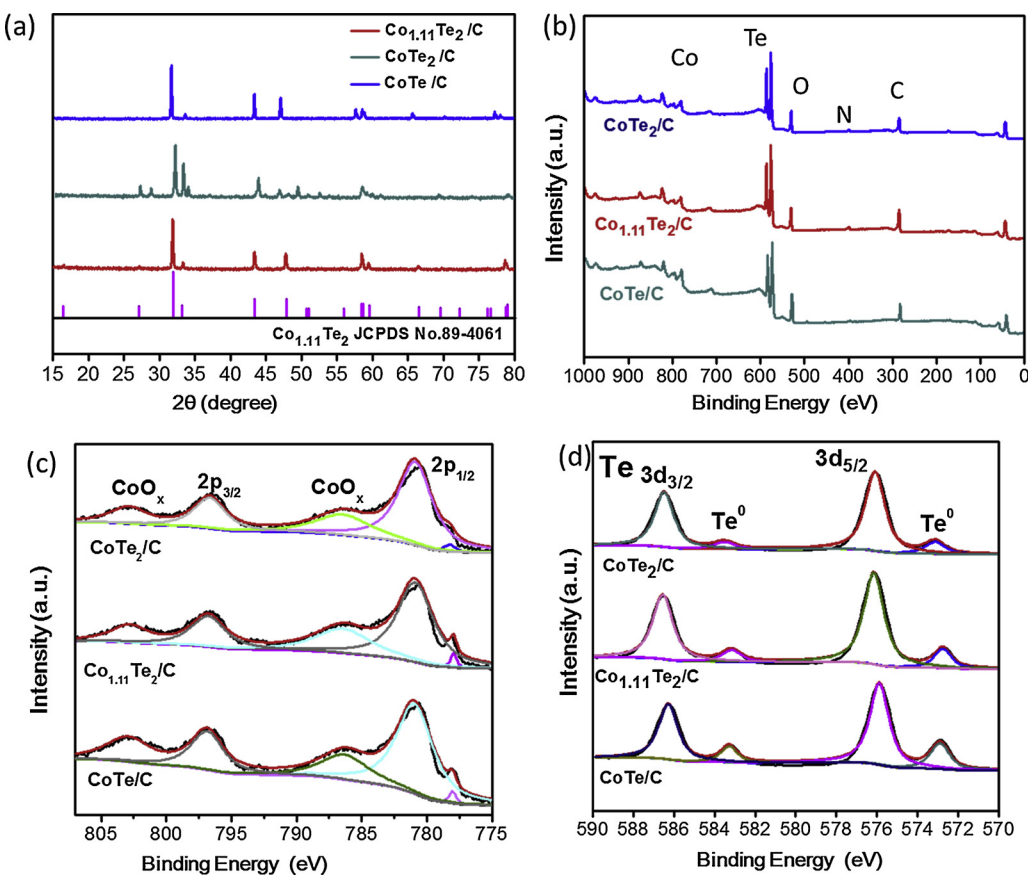
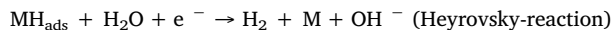
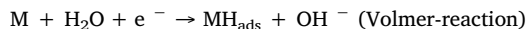


**Fig. 2.** (a) XRD patterns of Co<sub>1.11</sub>Te<sub>2</sub>/C, CoTe<sub>2</sub>/C and CoTe/C. (b) XPS survey spectra of CoTe<sub>2</sub>/C, Co<sub>1.11</sub>Te<sub>2</sub>/C and CoTe/C. High-resolution XPS spectra of (c) Co 2p and (d) Te 3d of CoTe<sub>2</sub>/C, Co<sub>1.11</sub>Te<sub>2</sub>/C and CoTe/C.

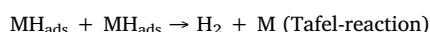
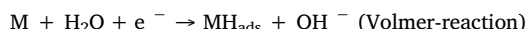
and large surface area of carbon templates ZIF-67, the anchored active Co<sub>1.11</sub>Te<sub>2</sub> could expose more active sites and provide more electron transfer access to promote the electrocatalytic performance. Otherwise, the N-doped carbon structure could improve the electron conductivity and avoid the agglomeration of catalytic nanoparticles during the long-term electrocatalytic process.

The Tafel plots of Co<sub>1.11</sub>Te<sub>2</sub>/C, CoTe<sub>2</sub>/C, CoTe/C and Pt/C are also measured to further investigate the HER kinetics. As is illustrated in Fig. 4c, Co<sub>1.11</sub>Te<sub>2</sub>/C exhibits the lowest Tafel slope of 77.3 mV dec<sup>-1</sup> among CoTe<sub>2</sub>/C (97.8 mV dec<sup>-1</sup>) and CoTe/C (115.1 mV dec<sup>-1</sup>), suggesting the fastest HER kinetics of Co<sub>1.11</sub>Te<sub>2</sub>/C in the electrocatalytic process. Generally, the HER is a multi-step reaction process that occurs on the surface of catalysts according to the classic mechanism theory reported previously [58]. The HER mechanism may go through two possible pathways in alkaline media [59].

The Volmer–Heyrovsky pathway:



Or the Volmer–Tafel pathway:



In theory, the determination of the rate-limiting step for HER is related to the value of the Tafel slope. Volmer, Heyrovsky and Tafel reaction correspond to a slope value of 120 mV dec<sup>-1</sup>, 40 mV dec<sup>-1</sup> and 30 mV dec<sup>-1</sup>, respectively [60]. Therefore, the Tafel slopes of Co<sub>1.11</sub>Te<sub>2</sub>/C, CoTe<sub>2</sub>/C, CoTe/C are all in the range of 40–120 mV dec<sup>-1</sup>, indicating that the HER mechanism over cobalt tellurium is functioned

by the Volmer–Heyrovsky pathway and the Heyrovsky step is the rate-limiting step. Furthermore, the electron-transport HER kinetics at the interface between the catalysts and electrolyte can be studied by the electrochemical impedance spectroscopy (EIS). Fig. 4d demonstrates the Nyquist plots of Co<sub>1.11</sub>Te<sub>2</sub>/C, CoTe<sub>2</sub>/C, CoTe/C, indicating that the charge resistance ( $R_{ct}$ ) value of Co<sub>1.11</sub>Te<sub>2</sub>/C is smallest in comparison with CoTe<sub>2</sub>/C and CoTe/C, matching the tendency of rising Tafel slopes of corresponding samples. Besides, the turnover frequency (TOF) is also a kinetic parameter for an electrochemical reaction process. And the TOFs of Co<sub>1.11</sub>Te<sub>2</sub>/C, CoTe<sub>2</sub>/C, CoTe/C were calculated by the following equation [61]:

$$TOF = (J \times A) / (2 \times F \times n)$$

In this equation, J represents the current density (A cm<sup>-2</sup>), A represents surface area of electrode (cm<sup>-2</sup>), 2 represents 2 electrons·mol<sup>-1</sup> of H<sub>2</sub>, F represents Faraday constant (96485 C), and n is number of moles of all Co ions or surface Co ions on the electrode. Firstly, the concentration of Co ions in the samples was measured by inductively coupled plasma atom emission spectrometry (ICP-AES) test (details can be seen in Table S1). All of the Co ions are postulated to be active sites, thereby the TOFs calculated by this method stand the average value. And the TOFs of Co<sub>1.11</sub>Te<sub>2</sub>/C, CoTe<sub>2</sub>/C and CoTe/C were counted to be 0.37, 0.18 and 0.018 H<sub>2</sub>/s at  $\eta = 400$  mV, respectively. But considering that some sites of cobalt are not available for HER process, the surface concentration of Co ions was calculated from H<sub>2</sub>-TPR results (Table S1) for comparison. According to this method, the TOF value of Co<sub>1.11</sub>Te<sub>2</sub>/C, CoTe<sub>2</sub>/C and CoTe/C was counted to be 10.76, 7.35 and 1.21 H<sub>2</sub>/s at  $\eta = 400$  mV, respectively, which is consistent with the order of values (Co<sub>1.11</sub>Te<sub>2</sub>/C > CoTe<sub>2</sub>/C > CoTe/C) obtained by the above calculation method. These results reveal that Co<sub>1.11</sub>Te<sub>2</sub>/C has the fastest electron transport rate to display the best electrocatalytic activities.

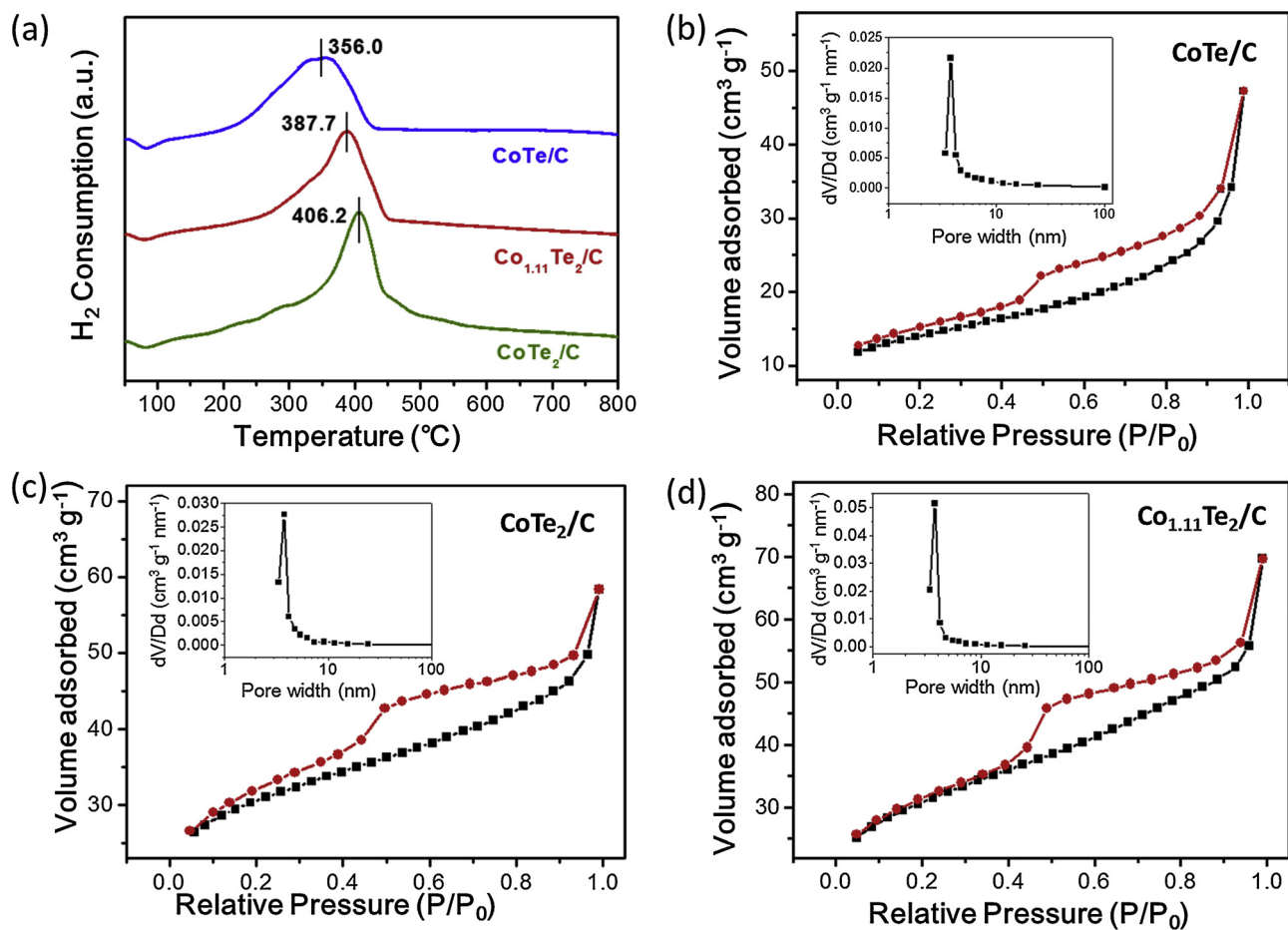


**Fig. 3.** (a) H<sub>2</sub>-TPR profiles of CoTe<sub>2</sub>/C, Co<sub>1.11</sub>Te<sub>2</sub>/C and CoTe/C. N<sub>2</sub> adsorption–desorption isotherms curves (insert is the corresponding pore size distribution of (b) CoTe/C, (c) CoTe<sub>2</sub>/C and (d) Co<sub>1.11</sub>Te<sub>2</sub>/C.

In order to further evaluate the great HER electrocatalytic activity of the synthesized electrocatalysts, electrochemically active surface areas were obtained based on testing the double layer capacitance ( $C_{dl}$ ). The cyclic voltammetry (CV) were measured in the potential range of 0.38 to 0.46 V (vs RHE) at the scan rate of 20, 40, 60, 80, 100, 120 mV s<sup>-1</sup> and the corresponding curves are shown in Fig. S11. Fig. 4e plots the differences of current density value at the middle scanning potential of the anodic and cathodic scan ( $J_{anodic} - J_{cathodic}$ ) versus the different scan rates, acquiring the linear trend. Through calculating the linear slope, we can obtain that the  $C_{dl}$  values of Co<sub>1.11</sub>Te<sub>2</sub>/C, CoTe<sub>2</sub>/C, CoTe/C are 64.8, 45.1, 18.9 mF cm<sup>-2</sup>, respectively. The fact that Co<sub>1.11</sub>Te<sub>2</sub>/C displays the largest  $C_{dl}$  value among the tested samples means Co<sub>1.11</sub>Te<sub>2</sub>/C possesses the largest active surface area, which may attribute to its unique electronic structure, offering more effective active sites. The above results demonstrate that Co<sub>1.11</sub>Te<sub>2</sub>/C has the best catalytic activity among the tested samples with different Co/Te ratio, which may be attributed to the unique electron structure of Co<sub>1.11</sub>Te<sub>2</sub>/C. The previous work reported by Yi Cui et al. claimed that the electrochemical performance of catalysts was related to the bonding mode and valence state of metals [62]. Yang Shao-Horn et al. have also found that d-electron configuration of cobalt might have great influence on the physical properties of catalysts [63]. Thus, the modification of Co/Te composition may adjust d bond electronic structure of the metal Co, further reducing the kinetic energy barrier of H–H bond formation on the surface of Co-based materials [64]. And Co<sub>1.11</sub>Te<sub>2</sub>/C might possess a near-optimal reaction free energy in comparison with others. What's more, during the calcination process, the structure defects of the carbon material will aggrandize with the increase of temperature, indicating that the defects of the carbon structure can afford more active sites and

enhance the HER performance more effectively at a higher temperature. But CoTe/C obtained at the highest temperature exhibits the poorest catalytic activity towards HER, which is due to the unoptimal electronic structure of CoTe/C. These results might prove that the composition is the main factor in affecting catalytic activities of the three as-prepared materials from one perspective.

What's more, high stability is also a very important factor in the evaluation of great HER performance. Firstly, to reveal the reversibility of the prepared catalyst, CV curves of the Co<sub>1.11</sub>Te<sub>2</sub>/C were cycled for 1000 cycles. The polarization curves before and after 1000 cycles are demonstrated in Fig. 4f, indicating that Co<sub>1.11</sub>Te<sub>2</sub>/C presents a good cycling performance with small performance loss. Moreover, the chronoamperometric test of Co<sub>1.11</sub>Te<sub>2</sub>/C was also performed at the constant current density of 10 mA cm<sup>-2</sup> for 20 h. After consecutively electrolyzing, only a small increase of overpotential can be observed. These results show that Co<sub>1.11</sub>Te<sub>2</sub>/C possesses great durability during the long-term electrocatalytic process. Importantly, as is listed in Table S2, the HER performance of Co<sub>1.11</sub>Te<sub>2</sub>/C is better than that of many other reported catalysts.

## 2.7. DFT calculations

Finally, DFT calculations were further conducted to rationalize the above experimental results (details can be seen in the supporting information). The simulated structure models of Co<sub>1.11</sub>Te<sub>2</sub>/C, CoTe<sub>2</sub>/C and CoTe/C are illustrated in Fig. 5a–c, respectively. For many catalysts in alkaline media, it is well accepted that the HER approach can be generalized for three states, which include the first catalyst-H<sub>2</sub>O status, the second catalyst-H<sup>+</sup> status and the final catalyst-H<sub>2</sub> status. Previous

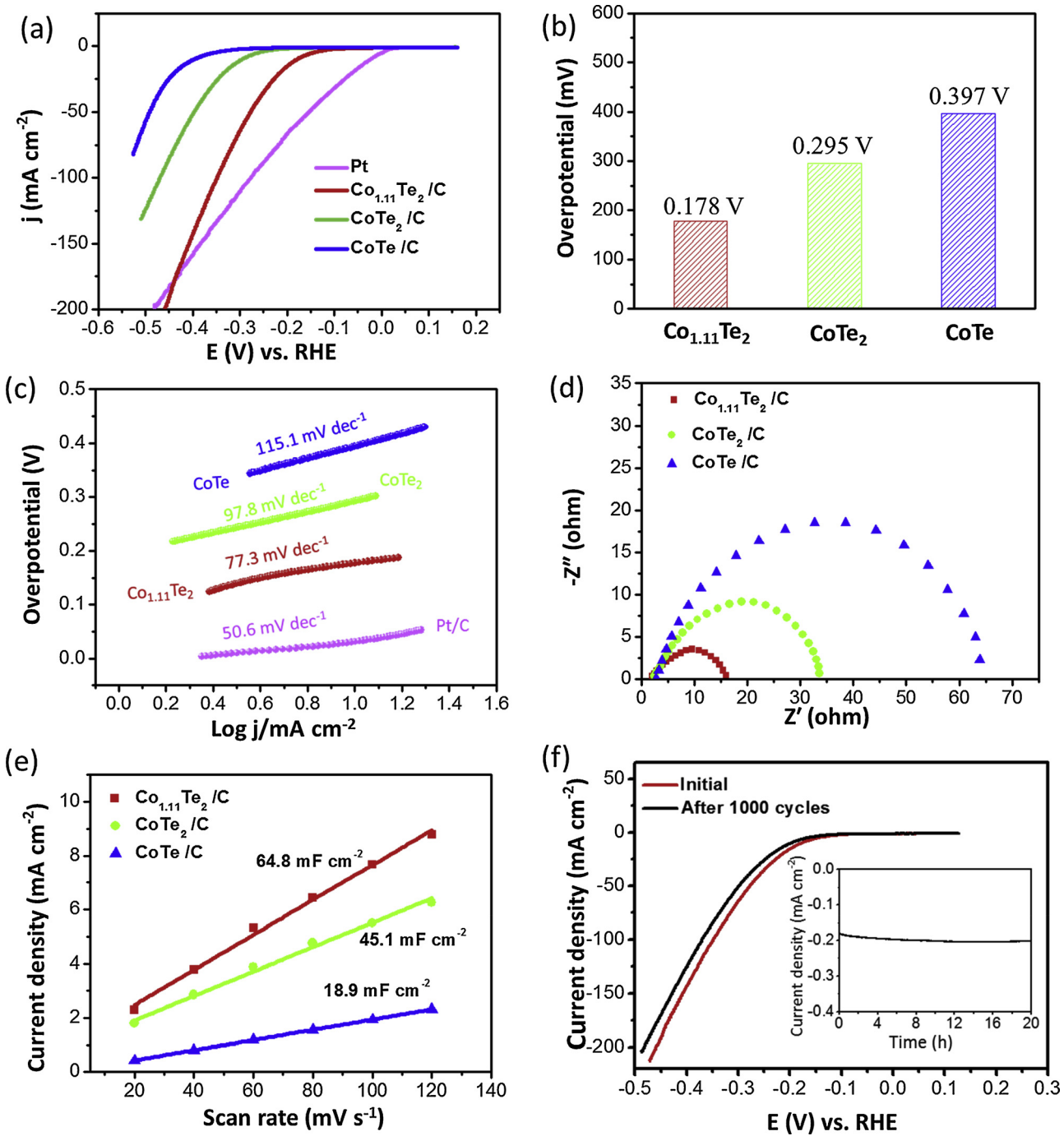


**Fig. 4.** (a) HER polarization curves of Co<sub>1.11</sub>Te<sub>2</sub>/C, CoTe<sub>2</sub>/C and CoTe/C and Pt/C in 1 M KOH. (b) overpotentials of Co<sub>1.11</sub>Te<sub>2</sub>/C, CoTe<sub>2</sub>/C and CoTe/C at the current of 10 mA cm<sup>-2</sup>. (c) Corresponding Tafel slopes of Co<sub>1.11</sub>Te<sub>2</sub>/C, CoTe<sub>2</sub>/C and CoTe/C. (d) Plots of the current density. (e) Nyquist plots. (f) CV curves of the Co<sub>1.11</sub>Te<sub>2</sub>/C catalyst before and after 1000 cycles and the insert showing chronoamperometric curves at the current of 10 mA cm<sup>-2</sup>.

reported works have proved that the suitable value of Gibbs free energy of catalyst–H\* ( $\Delta G_{H^*}$ ) is 0, where the adsorption and desorption of H\* at the electrocatalyst can be well balanced for H<sub>2</sub> production. Therefore, the  $\Delta G_{H^*}$  value of a catalyst could be reasonably applied to judge the catalytic performance for HER (the closer to the  $\Delta G_{H^*}$  value of 0, the better the HER performance). Based on that, we calculated  $\Delta G_{H^*}$  of Co<sub>1.11</sub>Te<sub>2</sub>/C, CoTe<sub>2</sub>/C and CoTe/C by building the relative theoretical models (Figs. S12–14). The calculated lattice parameters of as-prepared catalysts with experimental and theoretical comparison are illustrated in Table S3, and the space groups of Co<sub>1.11</sub>Te<sub>2</sub>/C, CoTe<sub>2</sub>/C and CoTe/C are P63/mmc, P-3m1 and Pmnn, respectively. Fig. 5d displays the computational Gibbs free energy diagram of Co<sub>1.11</sub>Te<sub>2</sub>,

CoTe<sub>2</sub> and CoTe (see Table S4 for more details). According to the calculated results, we can see that the  $\Delta G_{H^*}$  value of Co<sub>1.11</sub>Te<sub>2</sub> (−0.1202 eV) is very close to the ideal  $\Delta G_{H^*}$  value (0 eV) toward the catalyst–H\* state, suggesting the optimal H adsorption on the Co<sub>1.11</sub>Te<sub>2</sub> surface during the catalytic process for HER. Compared with Co<sub>1.11</sub>Te<sub>2</sub>, CoTe<sub>2</sub> and CoTe have larger  $\Delta G_{H^*}$  value, which are 0.1708 eV and 0.6148 eV, respectively, resulting in the weak adsorption of H\* that could cause the low HER activity of catalysts. The reason that Co<sub>1.11</sub>Te<sub>2</sub> possesses the optimal  $\Delta G_{H^*}$  in the HER process under alkaline condition among three catalysts may be attributed to its optimal electric structure, which can perform the best catalytic function. The order of  $|\Delta G_{H^*}|$  value of as-synthesized catalysts (Co<sub>1.11</sub>Te<sub>2</sub> < CoTe<sub>2</sub> < CoTe)

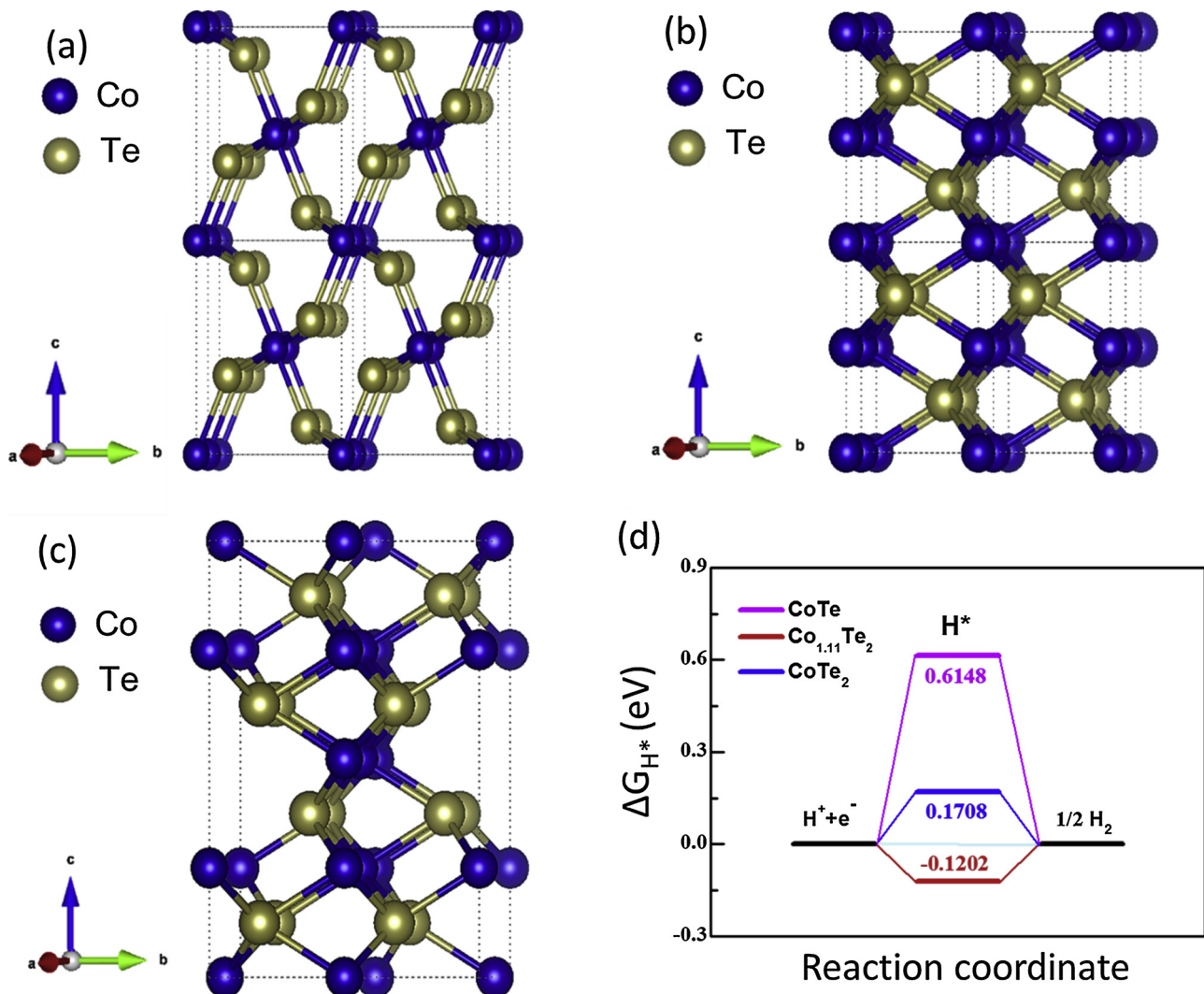


Fig. 5. The theoretical calculation models of (a)  $\text{CoTe}_2$ , (b)  $\text{CoTe}$  and (c)  $\text{Co}_{1.11}\text{Te}_2$ . (d) Gibbs free energy diagram of  $\text{CoTe}_2$ ,  $\text{Co}_{1.11}\text{Te}_2$  and  $\text{CoTe}$ .

verifies the experimental results (HER activity:  $\text{Co}_{1.11}\text{Te}_2 > \text{CoTe}_2 > \text{CoTe}$ ).

In summary, such good electrocatalytic activity of  $\text{Co}_{1.11}\text{Te}_2/\text{C}$ , which is investigated in this work for HER in alkaline conditions, might be ascribed to the several reasons as follows:

- (1) For cobalt tellurium, the 3d bands from Co ions, which can further split into  $t_{2g}$  and  $e_g$  sub-bands in the crystal field, adopt a low-spin coordination in the form of component [32,62,63]. That could make cobalt tellurium own the outstanding metallic characteristics and good electronic conductivity, further promoting the high electrocatalytic activity for HER.
- (2) Due to the porous characteristics and large surface area of carbon substrates, the anchored active cobalt tellurium nanoparticles could expose more active sites and provide more electron transfer access to promote the electrocatalytic performance. Otherwise, the N-doped carbon substrates could also improve the electron conductivity and avoid the agglomeration of catalytic nanoparticles during the long-term electrocatalytic process.
- (3) The modification of Co/Te composition may adjust d bond electronic structure of the metal Co, further reducing the kinetic energy barrier of H–H bond formation on the surface of Co-based materials [59]. And  $\text{Co}_{1.11}\text{Te}_2/\text{C}$  might possess a near-optimal reaction free energy, showing a higher catalytic activity in comparison with others.

(4) DFT calculations have been conducted to verify that  $\text{Co}_{1.11}\text{Te}_2$  possesses the optimal  $\Delta G_{H^*}$  value compared with  $\text{CoTe}_2$  and  $\text{CoTe}$ .

### 3. Conclusion

In summary, we have successfully synthesized the nitrogen-doped mesoporous graphitic carbon frameworks encapsulating component-modified cobalt telluride nanoparticles (including  $\text{CoTe}$ ,  $\text{Co}_{1.11}\text{Te}_2$  and  $\text{CoTe}_2$ ) using ZIF-67 as templates followed by the calcination process with adjusting the calcined temperature and the ratio of Co/Te. This N-doped graphitic carbon structure shows the merits of high surface area and great electric conductivity, thus enhancing the catalytic activity. Due to the structural and component advantages, the  $\text{Co}_{1.11}\text{Te}_2/\text{C}$  presents the highest catalytic activity for HER in 1M KOH compared with  $\text{CoTe}_2/\text{C}$ ,  $\text{CoTe}/\text{C}$  and  $\text{Co}_{1.11}\text{Te}_2$  powder. This work provides an effective strategy to prepare low-cost, environmental-friendly and efficient metal-based catalytic materials for HER and other related energy applications.

### Acknowledgements

This work was financially supported by the Fundamental Research Funds for the Central Universities (0301005202017, 2018CDQYFXCS0017, 106112017CDJXSYY0001), Thousand Young Talents Program of the Chinese Central Government (Grant No.

0220002102003), National Natural Science Foundation of China (NSFC, Grant No. 21373280, 21403019), Beijing National Laboratory for Molecular Sciences (BNLMS) and Hundred Talents Program at Chongqing University (Grant No. 0903005203205), The State Key Laboratory of Mechanical Transmissions Project (SKLMT-ZZKT-2017M11).

## Appendix A. Supplementary data

Supplementary material related to this article can be found, in the online version, at doi:<https://doi.org/10.1016/j.apcatb.2018.11.081>.

## References

- [1] P. Du, R. Eisenberg, *Energy Environ. Sci.* 5 (2012) 6012–6021.
- [2] Y. Jiao, Y. Zheng, M. Jaroniec, S.Z. Qiao, *Chem. Soc. Rev.* 44 (2015) 2060–2086.
- [3] L. Zhang, J. Lu, S. Yin, L. Luo, S. Jing, A. Brouzgou, J. Chen, P.K. Shen, P. Tsiaikaras, *Appl. Catal. B: Environ.* 230 (2018) 58–64.
- [4] H. Duan, D. Li, Y. Tang, Y. He, S. Ji, R. Wang, H. Lv, P.P. Lopes, A.P. Paulikas, H. Li, S.X. Mao, C. Wang, N.M. Markovic, J. Li, V.R. Stamenkovic, Y. Li, *J. Am. Chem. Soc.* 139 (2017) 5494–5502.
- [5] I. Roger, M.A. Shipman, M.D. Symes, *Int. Rev. Chem. Eng.* 1 (2017).
- [6] S. Jing, L. Zhang, L. Luo, J. Lu, S. Yin, P.K. Shen, P. Tsiaikaras, *Appl. Catal. B: Environ.* 224 (2018) 533–540.
- [7] A. Pirkarami, S. Rasouli, E. Ghasemi, *Appl. Catal. B: Environ.* 241 (2019) 28–40.
- [8] S.M. Tan, M. Pumera, *ACS Appl. Mater. Interfaces* 8 (2016) 3948–3957.
- [9] M.G. Walter, E.L. Warren, J.R. McKone, S.W. Boettcher, Q. Mi, E.A. Santori, N.S. Lewis, *Chem. Rev.* 110 (2010) 6446–6473.
- [10] Z. Pu, S. Wei, Z. Chen, S. Mu, *Appl. Catal. B: Environ.* 196 (2016) 193–198.
- [11] J. Tian, Q. Liu, A.M. Asiri, X. Sun, *J. Am. Chem. Soc.* 136 (2014) 7587–7590.
- [12] N. Bai, Q. Li, D. Mao, D. Li, H. Dong, *ACS Appl. Mater. Interfaces* 8 (2016) 29400–29407.
- [13] L.R.L. Ting, Y. Deng, L. Ma, Y.-J. Zhang, A.A. Peterson, B.S. Yeo, *ACS Catal.* 6 (2016) 861–867.
- [14] Y. Li, K. Yin, L. Wang, X. Lu, Y. Zhang, Y. Liu, D. Yan, Y. Song, S. Luo, *Appl. Catal. B: Environ.* 239 (2018) 537–544.
- [15] H.B. Wu, B.Y. Xia, L. Yu, X.Y. Yu, X.W. Lou, *Nat. Commun.* 6 (2015) 6512.
- [16] A.M. Gómez-Marín, E.A. Ticianelli, *Appl. Catal. B: Environ.* 209 (2017) 600–610.
- [17] S.K. Kim, Y. Qiu, Y.-J. Zhang, R. Hurt, A. Peterson, *Appl. Catal. B: Environ.* 235 (2018) 36–44.
- [18] G. Bellavance, L. Barriault, *Angew. Chem. Int. Ed.* 53 (2014) 6701–6704.
- [19] J.M. McEnaney, J.C. Crompton, J.F. Callejas, E.J. Popczun, A.J. Biacchi, N.S. Lewis, R.E. Schaak, *Chem. Mater.* 26 (2014) 4826–4831.
- [20] M.S. Faber, M.A. Lukowski, Q. Ding, N.S. Kaiser, S. Jin, *J. Phys. Chem. C Nanomater. Interfaces* 118 (2014) 21347.
- [21] X. Tang, X. Li, C. Yang, J. Lu, Z. Lin, *Int. J. Hydrogen Energy* 39 (2014) 3055–3060.
- [22] X. Wang, R. Su, H. Aslan, J. Kibsgaard, S. Wendt, L. Meng, M. Dong, Y. Huang, F. Besenbacher, *Nano Energy* 12 (2015) 9–18.
- [23] J. Li, Y.C. Wang, T. Zhou, H. Zhang, X.H. Sun, J. Tang, L.J. Zhang, A.M. Al-Enizi, Z.Q. Yang, G.F. Zheng, *J. Am. Chem. Soc.* 137 (2015) 14305–14312.
- [24] S. Emin, C. Altinkaya, A. Semerci, H. Okuyucu, A. Yildiz, P. Stefanov, *Appl. Catal. B: Environ.* 236 (2018) 147–153.
- [25] M.S. Faber, R. Dziedzic, M.A. Lukowski, N.S. Kaiser, Q. Ding, S. Jin, *J. Am. Chem. Soc.* 136 (2014) 10053–10061.
- [26] H. Zhang, B. Yang, X. Wu, Z. Li, L. Lei, X. Zhang, *ACS Appl. Mater. Interfaces* 7 (2015) 1772–1779.
- [27] J. McEnaney, T. Soucy, J. Hodges, J. Callejas, J. Mondschein, R.E. Schaak, *J. Mater. Chem. A* 4 (2016) 3077–3081.
- [28] X. Yan, L. Tian, M. He, X. Chen, *Nano Lett.* 15 (2015) 6015–6021.
- [29] K. Yin, Z.D. Cui, X.R. Zheng, X.J. Yang, S.L. Zhu, Z.Y. Li, Y.Q. Liang, *J. Mater. Chem. A* 3 (2015) 22770–22780.
- [30] P. Chen, K. Xu, S. Tao, T. Zhou, Y. Tong, H. Ding, L. Zhang, W. Chu, C. Wu, Y. Xie, *Adv. Mater.* 28 (2016) 7527–7532.
- [31] L.A. Stern, L. Feng, F. Song, X. Hu, *Energy Environ. Sci.* 8 (2015) 2347–2351.
- [32] X. Wang, X. Huang, W. Gao, Y. Tang, P. Jiang, K. Lan, R. Yang, B. Wang, R. Li, *J. Mater. Chem. A* 6 (2018) 3684–3691.
- [33] K. Wang, Z. Ye, C. Liu, D. Xi, C. Zhou, Z. Shi, H. Xia, G. Liu, G. Qiao, *ACS Appl. Mater. Interfaces* 8 (2016) 2910–2916.
- [34] T.-H. Lu, C.-J. Chen, M. Basu, C.-G. Ma, R.-S. Liu, *Chem. Commun.* 51 (2015) 17012–17015.
- [35] S.A. Patil, E.-K. Kim, N.K. Shrestha, J. Chang, J.K. Lee, S.-H. Han, *ACS Appl. Mater. Interfaces* 7 (2015) 25914–25922.
- [36] Q. Gao, C.-Q. Huang, Y.-M. Ju, M.-R. Gao, J.-W. Liu, D. An, C.-H. Cui, Y.-R. Zheng, W.-X. Li, S.-H. Yu, *Angew. Chem. Int. Ed.* 56 (2017) 7769–7773.
- [37] G. Wu, G. Cui, D. Li, P.-K. Shen, N. Li, *J. Mater. Chem.* 19 (2009) 6581–6589.
- [38] J. Jia, J. Wu, J. Dong, J. Lin, *Electrochim. Acta* 185 (2015) 184–189.
- [39] M.S. Khan, M.N. Ashiq, M.F. Ehsan, H. Tao, S. Ijaz, *Appl. Catal. A Gen.* 487 (2014) 202–209.
- [40] J. Guo, Y. Shi, Y. Chu, T. Ma, *Chem. Commun.* 49 (2013) 10157–10159.
- [41] M. Liu, Z. Wang, J. Liu, G. Wei, J. Du, Y. Li, C. An, J. Zhang, *J. Mater. Chem. A* 5 (2017) 1035–1042.
- [42] J.F. Callejas, C.G. Read, E.J. Popczun, J.M. McEnaney, R.E. Schaak, *Chem. Mater.* 27 (2015) 3769–3774.
- [43] N. Jiang, Q. Tang, M. Sheng, B. You, D.-e. Jiang, Y. Sun, *Catal. Sci. Technol.* 6 (2016) 1077–1084.
- [44] S. Damyanova, B. Pawelec, R. Palcheva, Y. Karakirova, M.C.C. Sanchez, G. Tyuliev, E. Gaigneaux, J.L.G. Fierro, *Appl. Catal. B: Environ.* 225 (2018) 340–353.
- [45] P. He, X.-Y. Yu, X.W. Lou, *Angew. Chem. Int. Ed.* 56 (2017) 3897–3900.
- [46] P. Zhang, B.Y. Guan, L. Yu, X.W. Lou, *Angew. Chem. Int. Ed.* 56 (2017) 7141–7145.
- [47] J. Tang, R.R. Salunkhe, J. Liu, N.L. Torad, M. Imura, S. Furukawa, Y. Yamauchi, *J. Am. Chem. Soc.* 137 (2015) 1572–1580.
- [48] N.L. Torad, R.R. Salunkhe, Y. Li, H. Hamoudi, M. Imura, Y. Sakka, C.-C. Hu, Y. Yamauchi, *Chem. Eur. J.* 20 (2014) 7895–7900.
- [49] Y. Gong, X. Zhao, H. Zhang, B. Yang, K. Xiao, T. Guo, J. Zhang, H. Shao, Y. Wang, G. Yu, *Appl. Catal. B: Environ.* 233 (2018) 35–45.
- [50] V. Ganesan, J. Kim, S. Radhakrishnan, *ChemElectroChem* 5 (2018) 1644–1651.
- [51] A.J. Reynoso, J.L. Ayastuy, U. Iriarte-Velasco, M.A. Gutiérrez-Ortiz, *Appl. Catal. B: Environ.* 239 (2018) 86–101.
- [52] X. Wang, J. Zhou, H. Fu, W. Li, X. Fan, G. Xin, J. Zheng, X. Li, *J. Mater. Chem. A* 2 (2014) 14064–14070.
- [53] F. Cao, M. Zhao, Y. Yu, B. Chen, Y. Huang, J. Yang, X. Cao, Q. Lu, X. Zhang, Z. Zhang, C. Tan, H. Zhang, *J. Am. Chem. Soc.* 138 (2016) 6924–6927.
- [54] Y. Zhang, A. Pan, L. Ding, Z. Zhou, Y. Wang, S. Niu, S. Liang, G. Cao, *ACS Appl. Mater. Interfaces* 9 (2017) 3624–3633.
- [55] Y. Tang, Z. Zhao, X. Hao, Y. Wang, Y. Liu, Y. Hou, Q. Yang, X. Wang, J. Qiu, *J. Mater. Chem. A* 5 (2017) 13591–13600.
- [56] Y. Ji, Z. Zhao, A. Duan, G. Jiang, J. Liu, *J. Phys. Chem. C* 113 (2009) 7186–7199.
- [57] W. Wei, H. Liang, K. Parvez, X. Zhuang, X. Feng, K. Müllen, *Angew. Chem. Int. Ed.* 53 (2014) 1570–1574.
- [58] V.M. Nikolic, S.L. Maslovava, G.S. Tasic, T.P. Brdaric, P.Z. Lausevic, B.B. Radak, M.P. Marceta Kaninski, *Appl. Catal. B: Environ.* 179 (2015) 88–94.
- [59] X. Gao, H. Zhang, Q. Li, X. Yu, Z. Hong, X. Zhang, C. Liang, Z. Lin, *Angew. Chem.* 128 (2016) 6398–6402.
- [60] M.A. Domínguez-Crespo, A.M. Torres-Huerta, B. Brachetti-Sibaja, A. Flores-Vela, *Int. J. Hydrogen Energy* 36 (2011) 135–151.
- [61] G. Zhang, G. Wang, Y. Liu, H. Liu, J. Qu, J. Li, *J. Am. Chem. Soc.* 138 (2016) 14686–14693.
- [62] D. Kong, H. Wang, Z. Lu, Y. Cui, *J. Am. Chem. Soc.* 136 (2014) 4897–4900.
- [63] J. Suntivich, K.J. May, H.A. Gasteiger, J.B. Goodenough, Y. Shao-Horn, *Science* 334 (2011) 1383.
- [64] Q. Gong, L. Cheng, C. Liu, M. Zhang, Q. Feng, H. Ye, M. Zeng, L. Xie, Z. Liu, Y. Li, *ACS Catal.* 5 (2015) 2213–2219.